NATIONAL ENERGY TECHNOLOGY LABORATORY

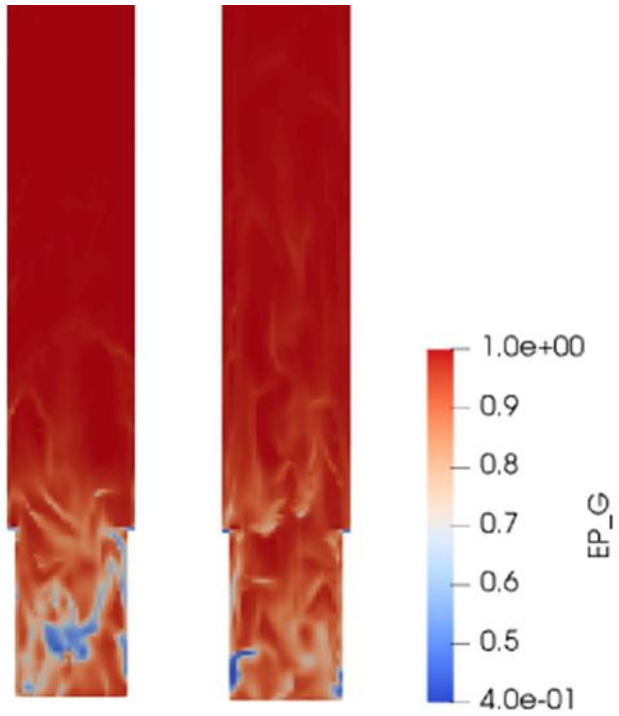

Computational Fluid Dynamics Analysis of a 12 MW Circulating Fluidized Bed Riser

15 October 2020

U.S. DEPARTMENT OF ENERGY | NATIONAL ENERGY TECHNOLOGY LABORATORY

Office of Fossil Energy

DOE/NETL-2020/2151

Disclaimer

This work was funded by the Department of Energy, National Energy Technology Laboratory, an agency of the United States Government, through a support contract with Leidos Research Support Team (LRST).

Cover Illustration: Contour plots of void fractions in the riser from the simulations: on the left is with monodisperse solid phase and on the right is with polydisperse solid phase. The concentration of gas phase is higher or the concentration of solids phase is lower in the bottom of the riser with monodisperse solid phase.

Suggested Citation: Chandramouli, D.; Shahnam, M.; Rogers, W. A. *Computational Fluid Dynamics Analysis of a 12 MW Circulating Fluidized Bed Riser*; DOE.NETL-2020.2151; NETL Technical Report Series; U.S. Department of Energy, National Energy Technology Laboratory: Morgantown, WV, 2020; p. 32. DOE: 10.2172/1673607.

Computational Fluid Dynamics Analysis of a 12 MW Circulating Fluidized Bed Boiler

Deepthi Chandramouli[1], Mehrdad Shahnam[2], William A. Rogers[2]

[1] U.S. Department of Energy, National Energy Technology Laboratory, Leidos Research Support Team, 3610 Collins Ferry Road, Morgantown, WV 26507

[2] U.S. Department of Energy, National Energy Technology Laboratory, 3610 Collins Ferry Road, Morgantown, WV 26507

DOE/NETL-2020/2151

15 October 2020

NETL Contacts:

William A. Rogers, Principal Investigator

Jonathan Lekse, Technical Portfolio Lead

Bryan Morreale, Executive Director, Research & Innovation Center

This page intentionally left blank.

Table of Contents

List of Figures

List of Tables

Acronyms, Abbreviations, and Symbols

Term	Description
2D	Two dimensional
3D	Three dimensional
CFB	Circulating fluidized bed
CFD	Computational fluid dynamics
MFiX	Multiphase Flow with Interphase eXchanges
NOx	Nitrogen oxides
PSD	Particle size distribution
SOx	Sulphur oxides
TFM	Two fluid model

Acknowledgments

This work was performed in support of the U.S. Department of Energy's (DOE) Fossil Energy Crosscutting Technology Research Program. The research was executed through the National Energy Technology Laboratory's (NETL) Research and Innovation Center's Advanced Reaction Systems Field Work Proposal. Research performed by Leidos Research Support Team staff was conducted under the RSS contract 89243318CFE000003.

ABSTRACT

A three-dimensional (3D) two fluid model (TFM) model of the 12 MW circulating fluidized bed (CFB) riser at Chalmers University was developed using the open-source Multiphase Flow with Interphase eXchanges (MFiX) Software Suite. The hydrodynamic behavior of the riser was validated by comparing axial pressure profiles from experimental measurements with the results from the simulations. Under some of the operating conditions where there was no external circulation of solids, the pressure profiles from the simulation matched well with the experimental measurements. For the cases where there was external circulation of solids, the pressure profiles with the monodisperse solid phase modeling underpredicted the solids concentration in the freeboard region. With the inclusion of polydispersity in the model, the predicted pressure profiles agreed well with the experimental measurements. A two-dimensional (2D) model of the riser was used to perform simulations of coal combustion. The predicted flue gas outlet compositions of oxygen and carbon dioxide compared reasonably to experiments. The experiments also reported some concentration of carbon monoxide which was overpredicted in the simulations. Additional experimental data such as axial oxygen concentration profile and pressure profiles were also compared with the experiment. It was observed that the oxygen concentration in the bottom bed from the simulations was higher than in the experiments, which suggested that most of the oxidation reactions occurred in the bottom bed. The concentration of volatiles and char in the simulations was lower in the bottom bed than in the experiments, which suggest that there is not sufficient penetration of the solid phase species into the bed.

1. INTRODUCTION

Circulating fluidized bed (CFB) technology has several advantages over traditional combustion techniques such as pulverized coal combustion. The most important of these is lower emissions such as nitrogen oxides (NOx) and sulphur oxides (SOx). Production of NOx is lower as a result of lower combustion temperatures, while SO_2 capture could be achieved by means of limestone addition. Another key advantage of the CFB is the ability to burn a range of fuels with varied size and shape ranges. This allows for cofiring of fuels such as coal and biomass (Blankinship, 2008). With increasing concerns about global warming, CFB allows for oxy fuel combustion thereby enabling CO_2 capture and sequestration.

Prediction of gaseous emissions from a CFB plant can be achieved with the assistance of computational fluid dynamics (CFD) modeling, which may further lead to optimized design of industrial scale units. In this study, a CFD analysis of the Chalmers 12 MW CFB system was performed. The Chalmers 12 MW CFB has a furnace of dimensions 13.5 m x 1.7 m x 1.4 m. A detailed description of the system is presented in the next section. To ensure the validity of the results from the model, a literature review was performed to obtain data from different tests performed on the 12MW CFB.

Amand et al. (1991) ran tests with bituminous coal at 12 MW capacity and reported measurements of CO_2, O_2, CO, and NO at the outlet of the furnace. They also reported concentration of O_2 along furnace riser. Amand et al. (1993) ran tests with two high-volatile bituminous coals from Poland. They ran tests to analyze the effect of lime addition on the NO/N_2O emissions and concluded that the emission of SO_2 itself influences the emissions of NO/N_2O from combustion. All tests were run at a constant load (9 MW). Amand et al. (1993) reported measurements of N_2O, NO, CO, and SO_2 in ppm using sand, lime, and a combination of sand and lime as bed materials. Johnsson and Leckner (1995) analyzed the vertical distribution of solids in the 12 MW CFB furnace. Wood pellet combustion was carried out using three sets of bed material and at varying inlet fluidizing gas velocities. The mean particle diameters of these sets were 440 microns, 320 microns, and 200 microns, as measured from the bottom bed. The inlet air velocities ranged between 1.3 m/s and 4.7 m/s. Johnsson and Leckner (1995) reported pressure measurements along the axis of the riser from these combustion experiments under seven operating conditions; they also estimated a solid circulation rate from the measured pressure profiles. Andersson (1996) measured local values of heat transfer to membrane walls of a circulating fluidized bed boiler for three size of silica sand with mean diameters of 0.22 mm, 0.34 mm, and 0.44 mm. They presented the particle size distribution (PSD) of a sample from the bottom bed as well as that of a sample from the cyclone return leg. Amand et al. (1999) carried out tests of combustion with three different fuels: bituminous coal, peat, and wood chips. They presented results of oxygen concentration profiles along the axis of the furnace. Leckner and Amand (2003) studied the emissions from co-combustion of coal, wood, and sludge. They reported measurements of emissions including NO, SO_2, CO, and N_2O under varying proportions of coal/sludge and wood/sludge mixtures. Nevalainen et al. (2007) reported measurements of oxygen concentration along the height of the riser with all coal, all wood, and a 50-50 mixture of wood and coal.

The remainder of this report is divided into three sections. The second section is focused on hydrodynamic validation, and discusses details of the experimental data, description of the model input, and the results from the hydrodynamic validation. The third section is focused on the modeling of the combustion process and compares key results from the simulations with the

experimental measurements. The last section presents a conclusion of the current study along with topics for future work.

2. HYDRODYNAMIC MODELING AND VALIDATION

2.1 SUMMARY OF EXPERIMENTAL DATA

Johnsson and Leckner (1995) analyzed the vertical distribution of solids in the 12 MW CFB boiler. The boiler has a furnace with dimensions 13.5 m x 1.7 m x 1.4 m, large enough to have most of the characteristics similar to commercial boilers. An outline of the boiler is shown in Figure 1.

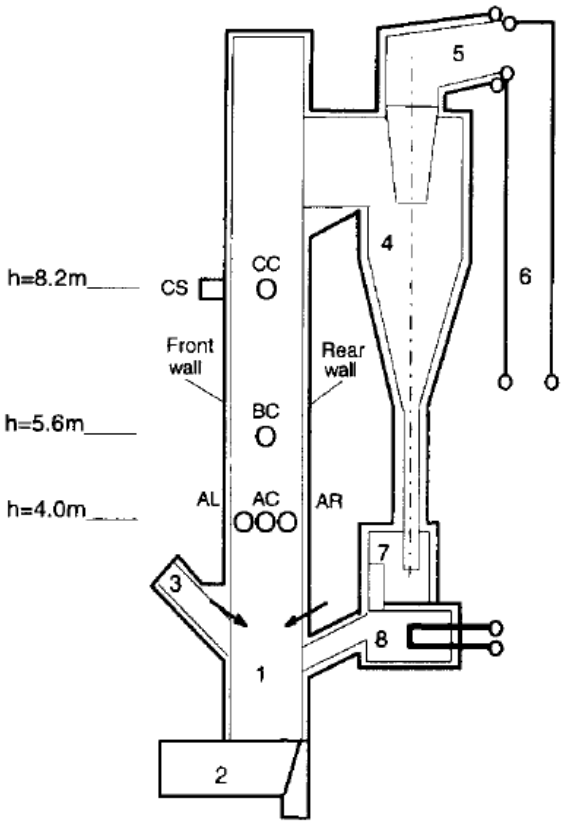

The 12 MW CFB boiler 1: combustion chamber; 2: air plenum and start-up combustion chamber; 3: fuel feed chute; 4: cyclone; 5: exit duct; 6: convection cooling section; 7: particle cooler; →: secondary air nozzles.

Figure 1: Outline of the CFB. Source: Zhang et al. (1995).

There are two vertical bare membrane tube walls that extend above a height of 2.2 m. The wall up to 2.2 m is covered by means of a refractory lining of 0.1 m thickness, resulting in an effective cross section of 1.5 m x 1.4 m in the bottom of the riser. The other walls are fully refractory lined.

Wood pellet combustion was carried out using silica sand as the inert bed material. Three silica sands with average particle size of 200 microns, 320 microns, and 440 microns were used. The PSD from the bottom bed at a height of 0.65 m is shown in Figure 2. The terminal velocities of the sands were 1 m/s, 2.1 m/s, and 3.3 m/s, respectively. The inlet air velocities ranged between

1.3 m/s and 4.7 m/s. Elutriated sand from the furnace was injected back to the bottom of the bed by means of a cyclone, standpipe, and a loop seal. Pressure measurements were recorded at 30 points along the axis of the furnace, shown in Figure 3. Based on the pressure profiles, three zones were identified with respect to the vertical distribution of solids in the furnace:

- **A bottom bed zone** with constant solids concentration
- **A splash zone** with an exponential decay in particle concentration with height and with a strong solids back mixing
- **A transport zone** also with an exponential decay in solids concentration but with a lower decay constant with solids back mixing mainly at the furnace walls

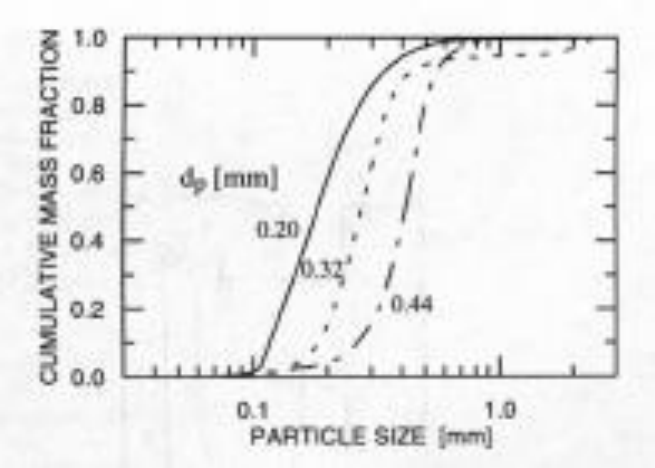

Figure 2: Particle size distribution from the experiments, sampled from the bottom bed material. Source: Johnsson and Leckner (1995).

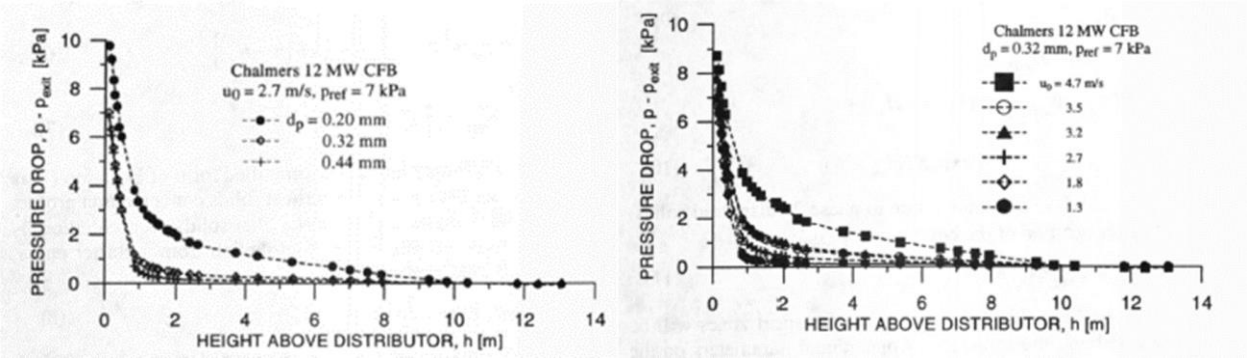

Figure 3: Axial pressure profiles. Source: Johnsson and Leckner (1995).

2.2 MODEL SET-UP

The MFiX two fluid model (TFM, Musser and Carney (2020)) suite was used to develop a three-dimensional (3D) model of the riser. The riser was modeled with a rectangular cross section of dimensions 13.5 m x 1.7 m x 1.5 m. The refractory lining up to a height of 2.2 m gave an effective cross section of 1.5 m x 1.4 m at the bottom. The inventory of sand in the riser was estimated from the pressure drop data. The circulation logic was achieved by means of user defined functions. The temperature of the fluidizing air was 850 °C.

The inventory of sand was specified as an initial condition. The fluidizing gas velocity at 850 °C was specified as a boundary condition. There was no secondary air injection. The furnace outlet was specified as a pressure outlet boundary condition. The elutriated solids mass flow rate from the furnace outlet was monitored and injected back from the bottom of the furnace as a mass inlet boundary condition. The simulations were run using variable time steps ranging between 1e-5 s and 1e-3 s. The cases with a monodisperse solid phase required 10 s–15 s of simulated time to reach steady state, whereas the cases with polydisperse solid phase required 20 s–25 s of simulated time to reach steady-state.

2.3 RESULTS WITH MONODISPERSE SOLID PHASE MODELING

The bed material was modeled as a monodisperse system with a diameter equal to the mean particle diameter of the bottom bed material as shown in Figure 2. The Gidaspow drag model was used. The grid size to particle size ratio used was 50.

Axial profiles of pressures along the riser from the simulations were compared with the experimental results. For the cases where there was no external circulation of solids, the results are presented in Figure 4 and Figure 5. Based on the pressure profiles, it was observed that the match to experimental pressures were good in the bottom bed zone. The agreement with the experimental pressures were reasonable in the splash zone. As the gas velocity is lower than the terminal velocity calculated based on the mean particle diameter, there is no clear presence of a transport zone. The behavior of the bed was similar to that of a turbulent fluidized bed.

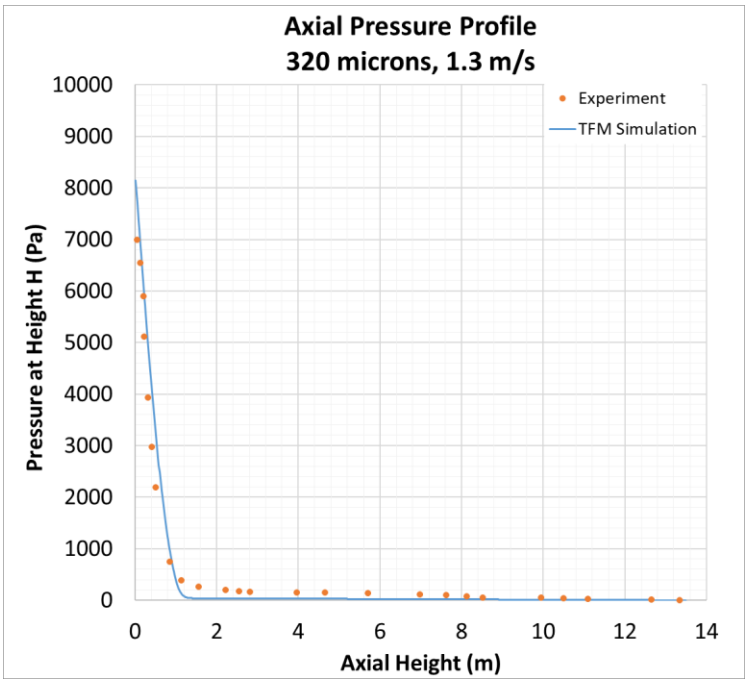

Figure 4: Results of axial pressure profiles with monodisperse solid phase modeling: 320 microns, 1.3 m/s.

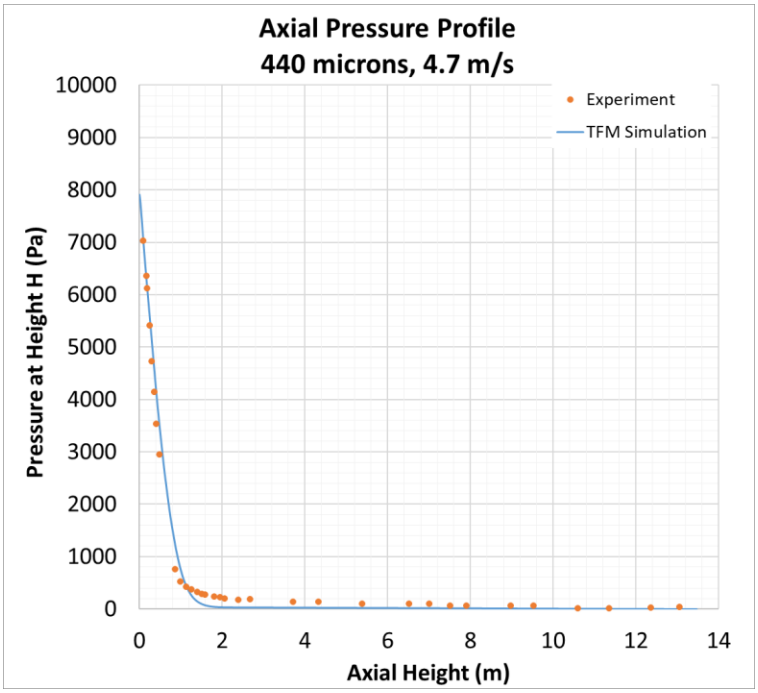

Figure 5: Results of axial pressure profiles with monodisperse solid phase modeling: 440 microns, 4.7 m/s.

The axial pressure profile for cases where there was external circulation of solids is shown in Figure 6 through Figure 9. The agreement in the pressure profile in the bottom bed zone is good. The simulations do predict a splash zone, but it occurs much higher in the riser when compared to the experiments. The simulations do not predict a defined transport zone. This may be due to the monodisperse modeling of the solid phase. The model is missing the variation in sizes of the bed material, particularly the finer material whose effect on pressure profile would be dominant in the transport zone.

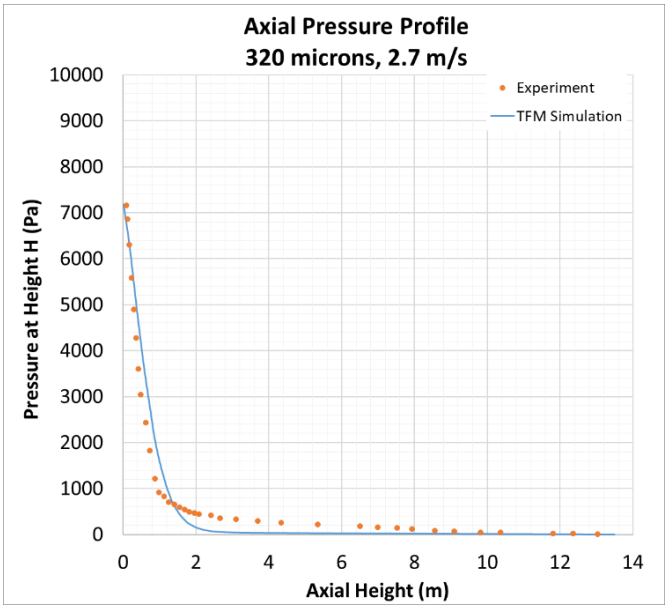

Figure 6: Results of axial pressure profiles with monodisperse solid phase modeling: 320 microns, 2.7 m/s.

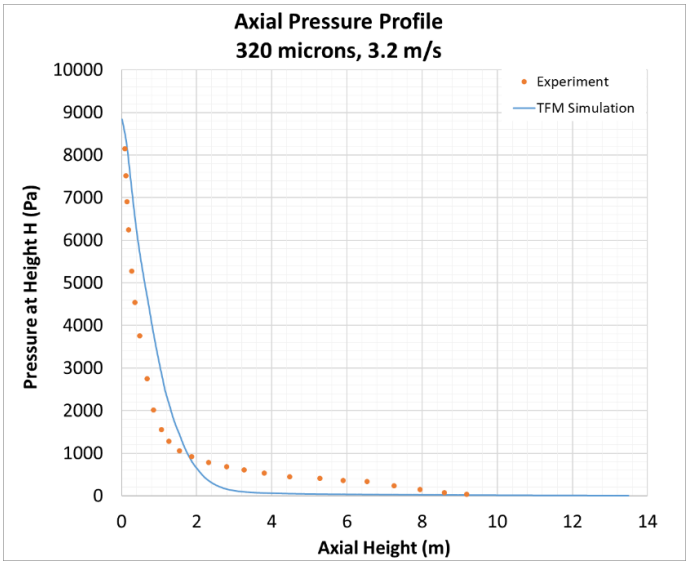

Figure 7: Results of axial pressure profiles with monodisperse solid phase modeling: 320 microns, 3.2 m/s.

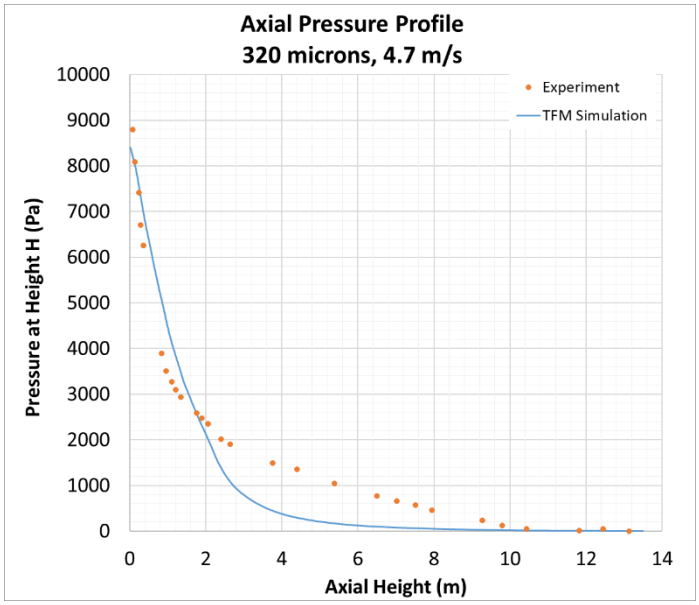

Figure 8: Results of axial pressure profiles with monodisperse solid phase modeling: 320 microns, 4.7 m/s.

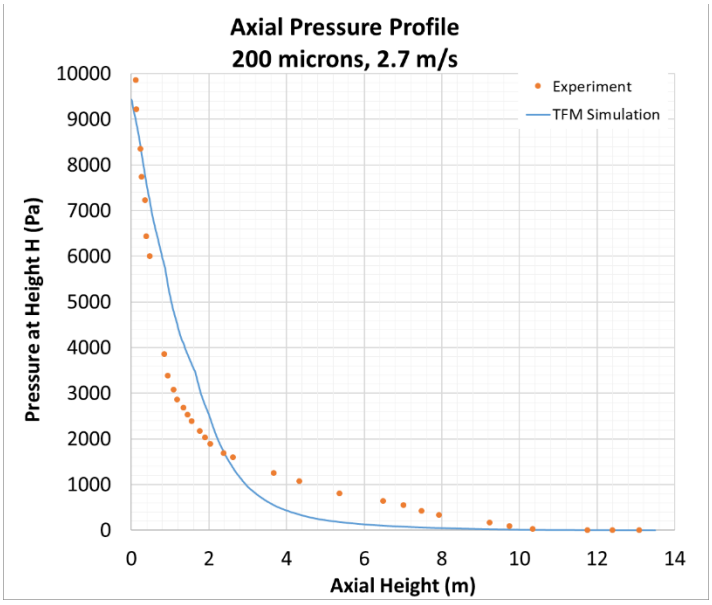

Figure 9: Results of axial pressure profiles with monodisperse solid phase modeling: 200 microns, 2.7 m/s.

2.4 RESULTS WITH POLYDISPERSE SOLID PHASE

The cases presented in Section 2.3 were modeled with a monodisperse assumption, where the Sauter mean diameter from the bottom bed material was used in the simulations. Some literature was available with information on particle size ranges in the other regions of the CFB, particularly from the cyclone which is representative of the circulated material. Table 1 shows the PSD sampled from the bottom 1.5 m of the bed and Table 2 shows the PSD of the circulated material sampled from the cyclone leg from Andersson (1996). The particle size from the cyclone leg was significantly smaller than the particle size in the bottom bed. For example, the mean diameter in the bottom bed for Case C was 220 microns, whereas the mean diameter of the circulated material was 96 microns, which is less than half the diameter of the bottom bed material. Therefore, the monodisperse cases set up with the Sauter mean diameter from the bottom bed may not be accurately representing the material in the full loop.

Table 1: PSD of the Bottom Bed Material. Source: Andersson (1996)

	Cumulative Mass Fraction									
Size (mm)	A	B	C	D	E	F	G	H	I	J
0.063–0.090	0.001	0	0.008	0.001	0.001	0.002	0.001	0.006	0.002	0
0.090–0.125	0.007	0.003	0.093	0.008	0.007	0.11	0.006	0.087	0.027	0.002
0.125–0.180	0.018	0.023	0.409	0.046	0.028	0.025	0.03	0.398	0.104	0.019
0.180–0.250	0.036	0.112	0.596	0.149	0.064	0.048	0.117	0.581	0.242	0.054
0.250–0.355	0.153	0.511	0.734	0.514	0.19	0.159	0.483	0.707	0.601	0.189
0.355–0.500	0.564	0.936	0.791	0.935	0.565	0.54	0.934	0.76	0.948	0.543
0.500–0.710	0.946	0.989	0.818	0.992	0.948	0.939	0.99	0.788	0.992	0.927
0.710–1.000	0.993	0.994	0.837	0.997	0.995	0.993	0.995	0.807	0.996	0.99
1.000–1.400	0.997	0.996	0.85	0.998	0.998	0.996	0.996	0.819	0.996	0.994
1.400–2.000	0.997	0.996	0.867	0.998	0.998	0.997	0.997	0.836	0.997	0.994
2.000–2.800	0.997	0.997	0.892	0.998	0.999	0.997	0.997	0.899	0.998	0.995
2.800–4.000	0.998	0.997	0.922	0.998	0.999	0.997	0.998	0.94	0.998	0.996
4.000–5.600	0.998	0.998	0.958	0.999	1	0.998	0.998	0.96	0.999	0.997
5.600–8.000	1	1	1	1	1	1	1	1	1	1
dp,mean	0.44	0.335	0.22	0.323	0.425	0.435	0.335	0.227	0.288	0.438

Table 2: PSD of the Circulated Material Sampled from the Cyclone Leg. Source: Andersson (1996)

Size (mm)	Cumulative Mass Fraction									
	A	B	C	D	E	F	G	H	I	J
<0.045	0.016	0.027	0.043		0.001	0.031	0.013	0.026		
0.045–0.063	0.047	0.039	0.098	0	0.001	0.061	0.017	0.057	0	0
0.063–0.090	0.258	0.141	0.325	0.018	0.008	0.261	0.106	0.226	0.009	0.002
0.090–0.125	0.726	0.45	0.744	0.18	0.067	0.655	0.379	0.676	0.115	0.022
0.125–0.180	0.936	0.765	0.969	0.396	0.189	0.862	0.645	0.963	0.311	0.1
0.180–0.250	0.977	0.929	1	0.622	0.29	0.924	0.849	1	0.511	0.199
0.250–0.355	0.997	0.996		0.889	0.476	0.975	0.981		0.811	0.387
0.355–0.500	1	1		0.996	0.792	0.997	0.999		0.986	0.725
0.500–0.710				1	0.984	1	1		0.999	0.972
0.710–1.000					0.999				1	0.999
1.000–1.400					1					1
dp,mean	0.103	0.124	0.096	0.187	0.276	0.106	0.138	0.104	0.211	0.33

For the same cases discussed in Section 2.3, the polydispersity in the solid phase was modeled using the information from Table 1 and Table 2. The solid phase in the model was specified using fifteen size bins. It was assumed that half of the total material in the entire loop had a PSD corresponding to the bottom bed and the remaining half corresponded to the PSD of the circulated material. The default parameters in MFiX were used to model the solid-solid momentum exchange. To model the multiple phases, a coarser grid was used to achieve reasonable computational speeds. A subgrid drag model (Gao et al., 2018) was used as result of the coarser grid. The results are shown in Figure 10 through Figure 13. It was observed that the prediction in the pressure profiles had improved significantly, and the simulations were able to predict the three regions (bottom bed zone, splash zone, and transport zone) clearly. The match to experiments was good.

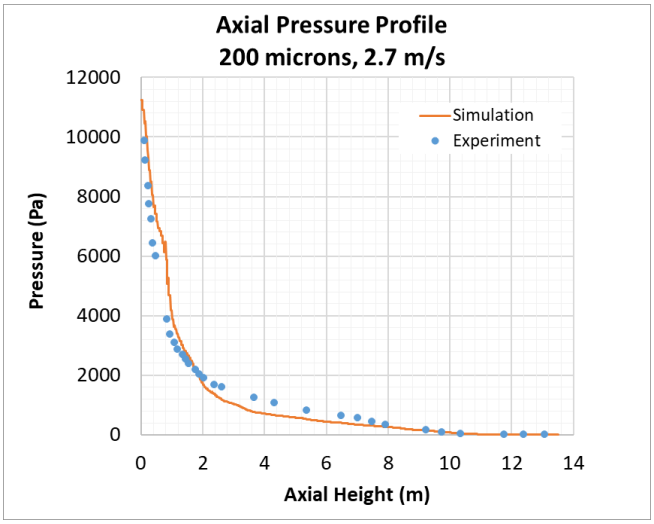

Figure 10: Results of axial pressure profiles with polydisperse solid phase modeling: 200 microns, 2.7 m/s.

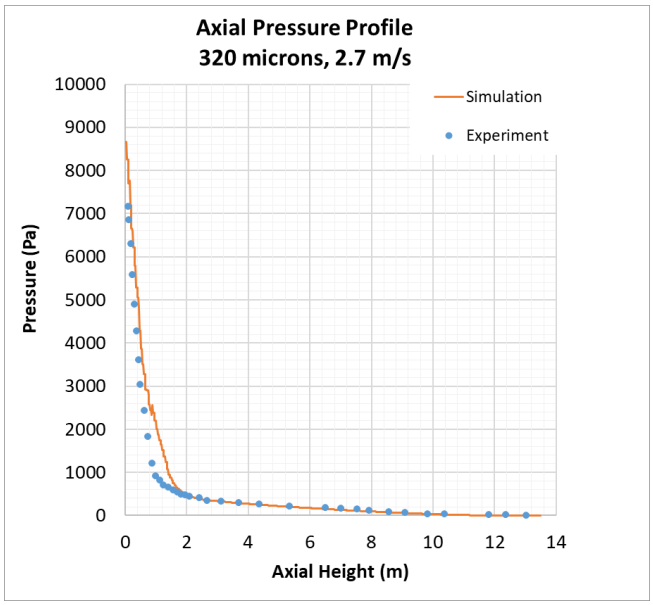

Figure 11: Results of axial pressure profiles with polydisperse solid phase modeling: 320 microns, 2.7 m/s.

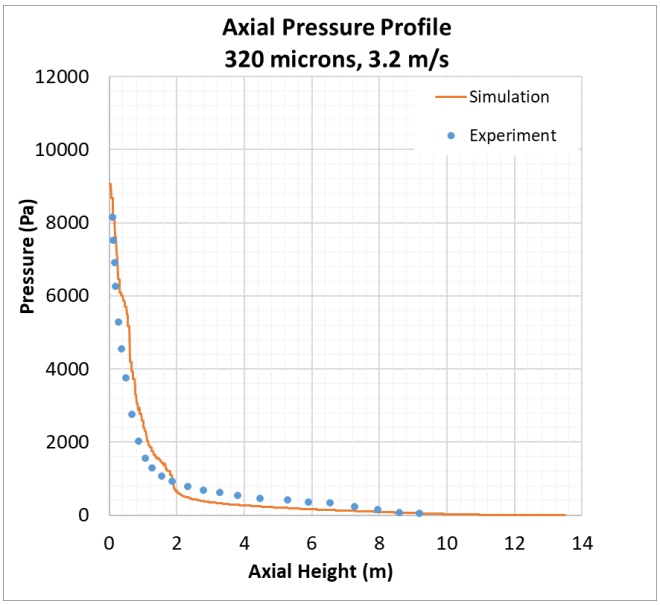

Figure 12: Results of axial pressure profiles with polydisperse solid phase modeling: 320 microns, 3.2 m/s.

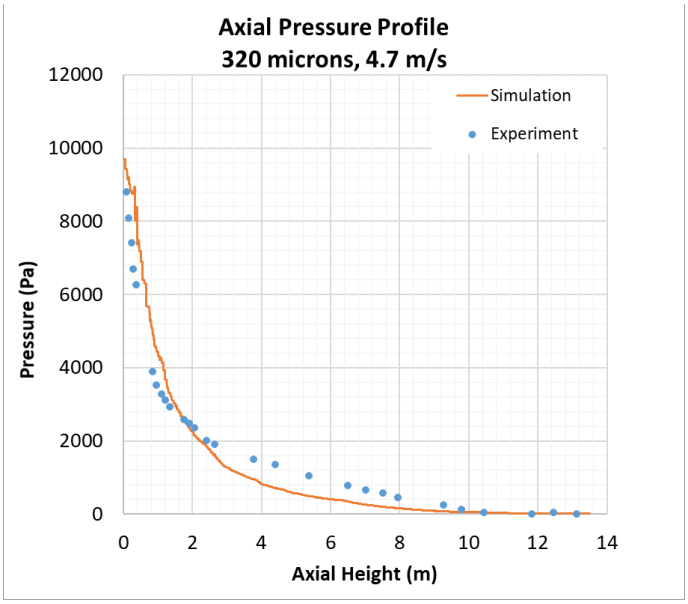

Figure 13: Results of axial pressure profiles with polydisperse solid phase modeling: 320 microns, 4.7 m/s.

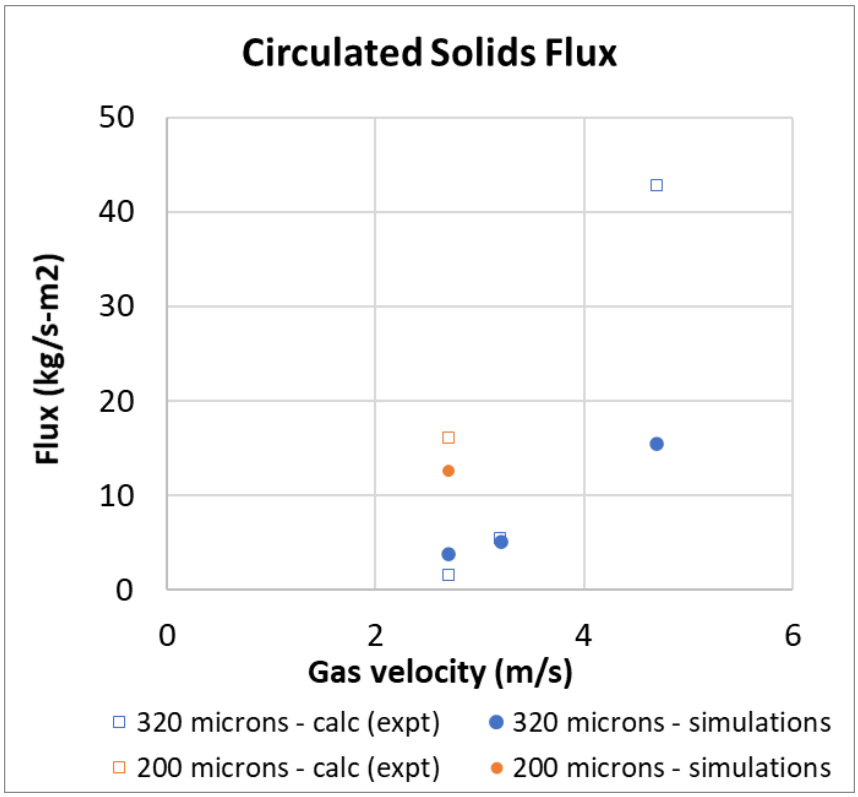

Figure 14: Circulated solids flux plotted against fluidizing gas velocity.

3. COMBUSTION MODELING AND VALIDATION

A two-dimensional (2D) model was used to simulate the combustion experiments conducted in the 12 MW Chalmers CFB. The results from the model were compared with coal combustion experimental data from Amand et al. (1991) and Amand et al. (1999). Amand et al. (1991) reported measurements of flue gas composition (oxygen, carbon dioxide, carbon monoxide, and NOx). The fuel used was bituminous coal, the proximate and ultimate analysis are shown in Table 3. The size of the coal particle was 0–30 mm with a mean size on a mass basis of 11 mm, and 13% of the fuel had a size less than 1 mm. Two operating conditions from Amand et al. (1991) were used for validating the results from the model. The excess air ratio and the primary air stoichiometry were different between the two conditions, as presented in Table 4. Amand et al. (1999) conducted experiments of coal combustion with a bituminous coal of a different composition, as outlined in Table 3. The mean particle size from the fuel feed was 8.5 mm. Amand et al. (1999) reported measurements of axial pressure profile, axial oxygen concentration profile, and axial distribution of char in the riser.

3.1 MODEL SET UP

MFiX TFM was used to model the reacting flow simulations. The inert bed material, sand, was modeled as a monodisperse solid phase. The reacting phase, coal was also modeled as a monodisperse solid phase with four species: char, volatiles, moisture, and ash. The compositions of these species were obtained from the proximate analysis of the fuel. The Gidaspow drag model (Ding and Gidaspow, 1990) was used to model the gas-solid momentum exchange. The default settings in MFiX were used for the solid-solid momentum exchange. The default settings include a granular energy algebraic formulation for the solid phase stress model, the Schaeffer model for the solids stress friction, and the Lebowitz radial distribution function (Musser and Carney, 2020). The fuel feed rate was calculated based on the primary air velocity, the excess air ratio, and the ultimate analysis.

The size of grid for cases 1 and 2 was 0.022 m, and the size of grid for case 3 was 0.016 m. The inventory of the inert material is specified as the initial condition. The fluidizing gas (air) is supplied from the bottom of the riser as a velocity boundary condition. The fuel is fed into the riser through a side inlet at 2.2 m above the distributor as a mass inlet boundary condition. Negligible purge gas volume is used at the fuel injection. There is secondary air injection in two of the cases, this was achieved by means of a volumetric boundary condition at 2.2 m above the distributor plate. The simulations were run with a variable time step in the range 1e-5 s to 1e-3 s for 120 s.

Table 3: Proximate and Ultimate Analysis

Fuel	Ultimate Analysis (%)					Proximate Analysis (%)			
	S	H	C	O	N	Char	Volatile	Moisture	Ash
Coal1	0.5	5	84	9	1.5	54.60	23.40	12.50	9.50
Coal2	1.84	5.5	78.4	12.7	1.6	44.52	29.68	16.90	8.90

Table 4: Operating Parameters Modeled

Case #	Case 1	Case 2	Case 3
Fuel	Coal1	Coal1	Coal2
Inert material	Sand - 440 microns (assumed)		Sand - 320 microns
Primary air velocity (m/s)	6	6	3.8
Primary air stoichiometry	0.75	1	0.65
Excess air ratio	1.2	1.3	1.2
Calculated fuel feed rate (kg/s)	0.55	0.39	0.43
Primary and secondary air inlet temperature (K)	1123 K		
Fuel inlet temperature (K)	1123 K		

The reactions modeled are comprised of drying, devolatilization, gasification and combustion (oxidation) reactions. A list of reactions is shown in Table 5. An Arrhenius rate was specified for the drying mechanism. The kinetics of pyrolysis and gasification were obtained from Li et al. (2017). The kinetics of carbon monoxide combustion and methane combustion were obtained from Westbrook and Dryer (1981). The kinetics of hydrogen combustion was obtained from Peters (1979).

Table 5: Reactions Modeled

#	Description	Reaction	Reaction Rate
1	Drying	Moisture → H_2O	$r_{drying} = 2 \times 10^{19} e^{\frac{-4571}{8.314T_C}} \frac{m_{c,m}}{MW_{c,m}}$
2	Pyrolysis	Volatile → 0.3 CO + 0.343 CO_2 + 0.051 H_2 + 0.278 CH_4 + 0.785 H_2O	$r_{pyrolysis} = 57.21 \times e^{\frac{-4571}{8.314T_c}} \frac{m_{c,v}}{MW_{c,v}}$
3	Char combustion	2 Char + O_2 → 2 CO	$r_{char} = \frac{p_{O_2} S_{char}}{MW_{O_2}\left[\frac{1}{k_{film}} + \frac{1}{k_{reaction}}\right]}$
4	Methane combustion	CH_4 + 2·O2 → CO_2 + 2 H_2O	$r_{CH_4} = 6.70 \times 10^{12} e^{\frac{-24360}{T_g}} c_{O_2}^{1.3} c_{CH_4}^{0.2}$
5	CO combustion	CO + 0.5·O_2 → CO_2	$r_{CO} = 3.98 \times 10^{14} e^{\frac{-2013}{T_g}} c_{O_2}^{0.25} c_{CO} c_{H_2O}^{0.5}$
6	Hydrogen combustion	H_2 + 0.5·O_2 → H_2O	$r_{H_2} = 1.08 \times 10^{16} e^{\frac{-15098}{T_g}} c_{O_2} c_{H_2}$
7	Steam Gasification	C + H_2O → CO + H_2	$r_{SG} = k_{SG1} e^{\frac{E_{SG}}{RT_g}} \frac{p_{H_2O}^{NAPP_{SG}}}{\left[1 + k_{SG2} p_{H_2}\right]} \frac{m_{c,c}}{MW_{c,c}}$
8	CO_2 Gasification	CO_2 + Char → 2 CO	$r_{CG} = k_{CG1} e^{\frac{E_{CG}}{RT_g}} \frac{p_{CO_2}^{NAPP_{CG}}}{\left[1 + k_{CG2} p_{CO_2}\right]} \frac{m_{c,c}}{MW_{c,c}}$

3.2 RESULTS

The outlet mole fractions of oxygen and carbon dioxide from the model were compared against experimental measurements. A reasonable match was obtained from the model as seen in Figure 15. Oxidation is slightly over-predicated in case 1 and slightly under-predicted in cases 2 and 3.

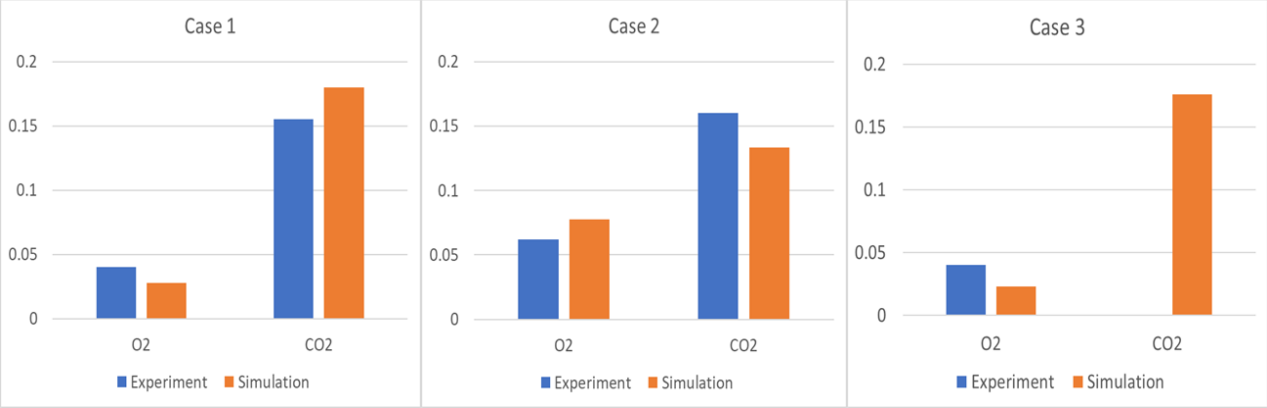

Figure 15: Flue gas composition – O_2 and CO_2.

Snapshots of rates of reactions (in k-mol/s-m^3), shown in Figure 16 through Figure 18 below, indicate the regions where and the extent to which the different reactions occur. Figure 16 shows the rates of devolatilization and char combustion. Devolatilization occurred at the inlet of coal. All volatile content in the fuel very quickly converted to the product gases and the volatile concentration in the combustor was depleted downstream of the inlet. Figure 17 shows rates of steam and CO_2 gasification reactions, these are much smaller in magnitude than char combustion. This indicates that char combustion was the most dominant among other reactions involving char, as expected. The experiments reported that 80% of the total mass of char in the riser was confined to the bottom 2 m. The simulations showed that 80% of the char concentration was in the bottom 3 m of the riser. One of the factors that may be causing this difference could be the solid-solid momentum exchange calculation. Additionally, the 2D modeling approach taken could also be causing some differences in the results. The homogenous gas phase combustion reactions occur mostly in the freeboard region, as shown in Figure 18. Most of these gases are formed as products of devolatilization, and therefore, are confined to the freeboard. These gases are the product of coal pyrolysis and char oxidation and gasification. Contours of oxygen mass fraction and gas phase temperatures are presented in Figure 19.

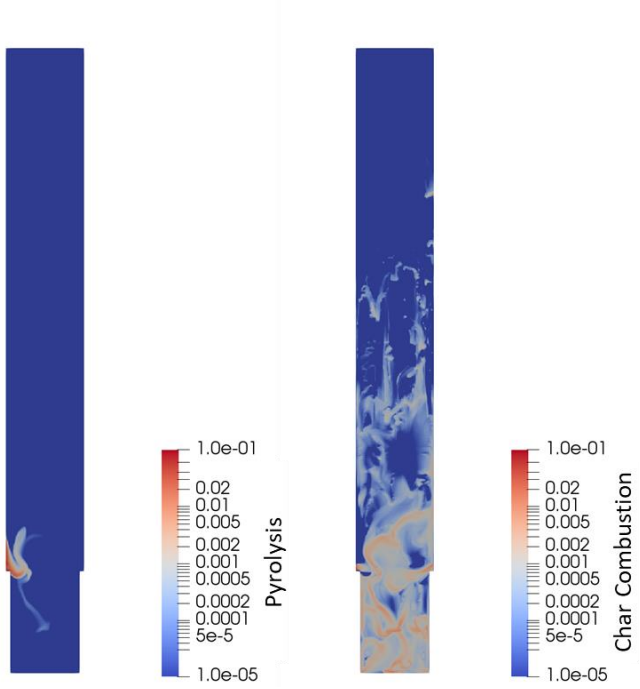

Figure 16: Contours of reaction rates of devolatilization and char combustion reactions.

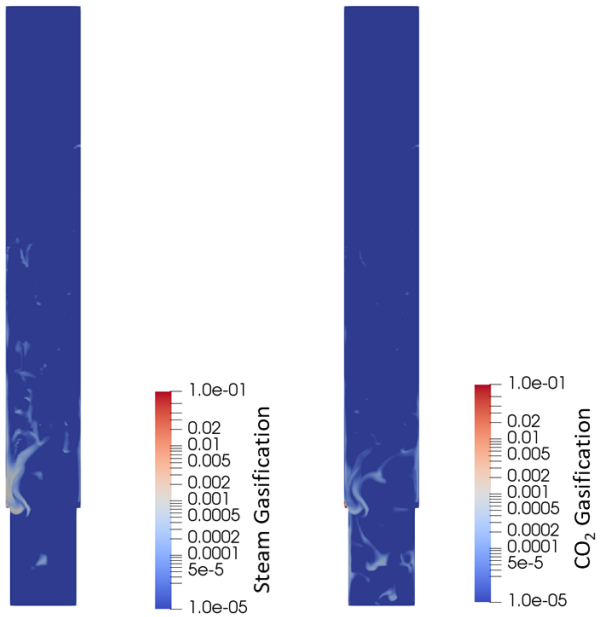

Figure 17: Contours of reaction rates of steam and CO_2 gasification.

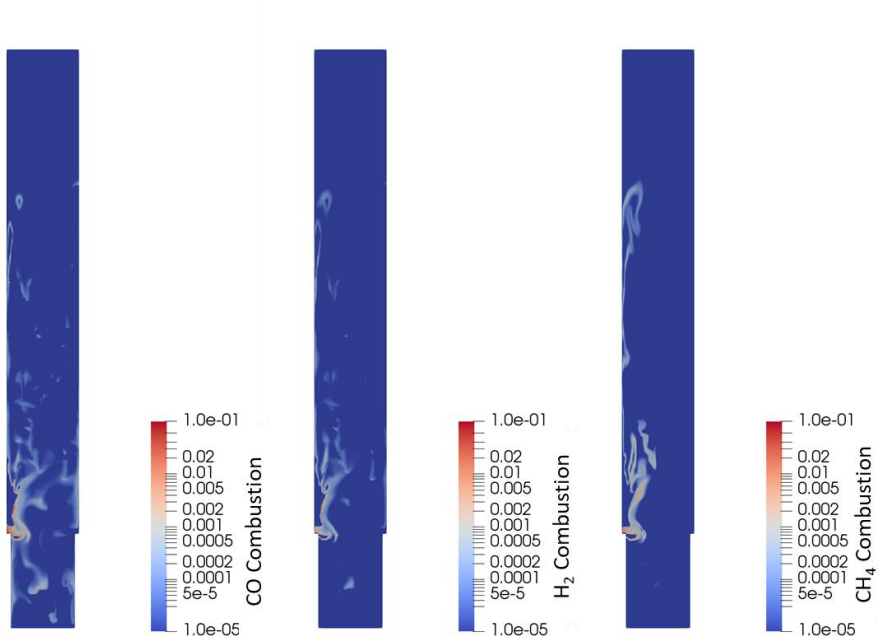

Figure 18: Contours of homogeneous gas phase combustion reaction rates.

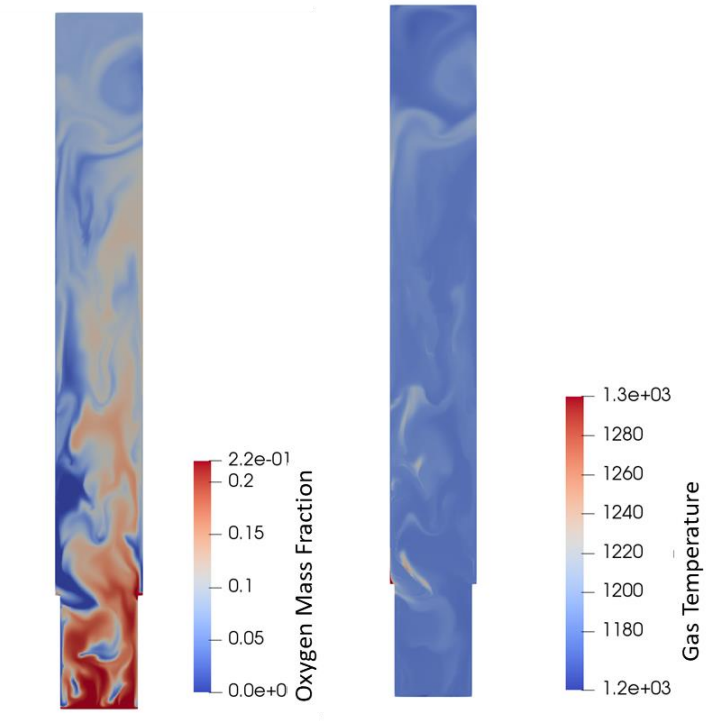

Figure 19: Contours of oxygen mass fraction and gas temperatures.

The axial pressure profile, centerline oxygen concentration profile, and some temperature measurements were reported by Amand et al. (1999) for case 3. The axial pressure profile is shown in Figure 20. The results were similar to those presented in Section 2.3, the offset from the experimental results is primarily due to the use of monodisperse sand particles and possibly coal particles in the reacting flow simulations. The oxygen concentration profiles along the centerline of the riser from the experiment and the simulations are shown in Figure 21. It should be noted that the oxygen concentration profiles from the experiments are unique in the case of the Chalmers CFB. The profiles show large variations over the cross section, explained as an effect of insufficient penetration of secondary air in combination with partial plugging of some of the secondary air nozzles. Despite the insufficient penetration, the oxygen concentration levels in the bottom of the riser (<1 m) are lower in comparison with the prediction. This indicates that most of the oxidation reactions occur <1 m of the riser in the experiments. In the simulations, it was observed that almost all of the homogenous (gas phase combustion) reactions occur in the freeboard region predominantly (Figure 18), and this contributes to higher oxygen levels at the bottom of the bed. The axial temperature profile is shown in Figure 22. It was observed that the temperatures are increasing along the height. In the experiments, the temperature reported at the top of the riser was very close to the bottom bed temperature. As the model is missing the heat transfer to walls, the temperatures in the model were higher.

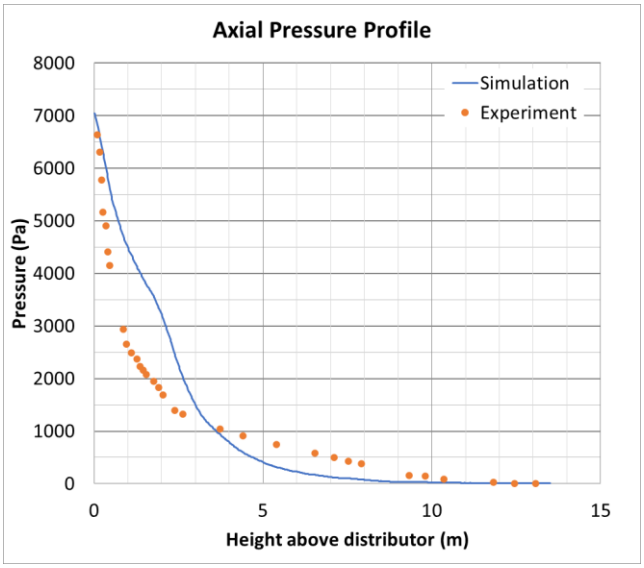

Figure 20: Axial pressure profile for case 3.

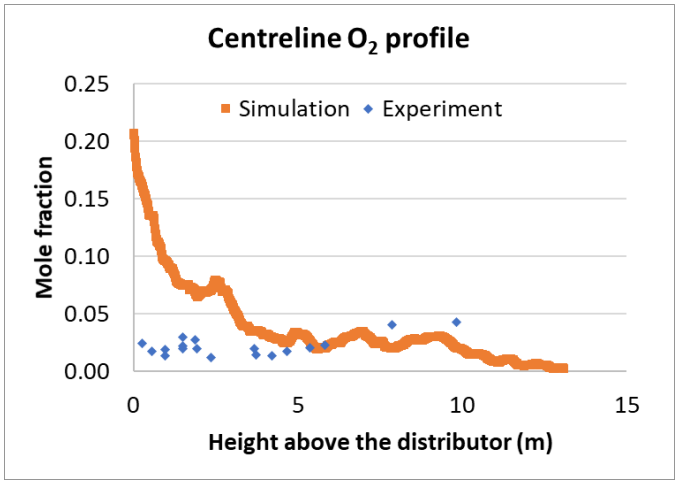

Figure 21: Axial O_2 profile along the centerline of the riser.

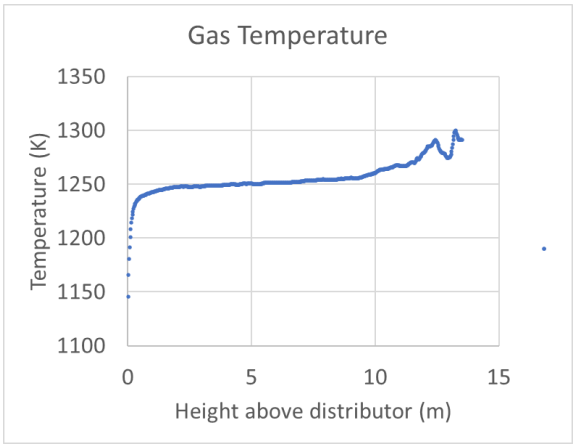

Figure 22: Axial temperature profile from the simulation.

4. CONCLUSIONS AND FUTURE WORK

The validation of the 12 MW system was done in two phases—a 3D model was developed for hydrodynamic validation and a 2D model was developed for validating combustion modeling. For the hydrodynamic validation, pressure profiles from the simulations were compared with experimental measurements. With monodisperse solid-phase modeling, the pressure profile matched well under operating conditions where there was no external circulation of the bed material. For cases with external circulation of bed material, the predicted pressure drop matched well in the bottom bed zone, but the match in the freeboard region needed additional investigation. When the solid phase was modeled as a polydisperse phase with fifteen size bins, the match in the pressure profile improved significantly. The match to experiments was good. The predicted circulation rates also aligned well with experimental calculations in most of the cases.

A 2D modeling approach was used for validating the combustion model. With the schemes currently used, the match to experiments for the outlet flue gas composition for oxygen and carbon dioxide was reasonable. The carbon dioxide concentration was overpredicted by the model. The predicted centerline oxygen concentration profiles along the axis of the riser compared with the experimental measurements. It was observed that the oxygen concentration in the bottom bed region was higher in the simulations as most of the oxidation reactions occur in the freeboard region. Additionally, experiments observed 80% concentration of char in the bottom 2 m, while in the simulations, 80% of the total mass of char was confined to the bottom 3 m of the riser. The temperature at the top of the riser is higher than the value reported in the experiments, one of the main reasons is the missing heat transfer modeling with the walls. Future work includes enhancements to the current modeling approach, some of which are identified below.

- Solid-solid momentum exchange: The higher oxygen levels in the bottom bed are linked to insufficient penetration of solid phase species (volatiles, char, and moisture) to the bottom of the bed. Modification to the solid-solid momentum exchange calculations may be necessary to address solids mixing. Additionally, the PSD of the coal particles is also needed.
- Alternate combustion kinetic schemes: Alternate combustion schemes could be employed to see if the prediction of O_2/CO_2 could be improved. Additional models for SO_2 and NOx prediction need to be identified and implemented for a more comprehensive validation.
- Heat transfer: The reactor consists of tube membrane walls on two sides. The convective heat transfer with the walls should be modeled.

This page intentionally left blank.

5. REFERENCES

Amand, L. E.; Leckner, B.; Andersson, S. Formation of N_20 in Circulating Fluidized Bed Boilers. *Energy & Fuels* **1991,** 815–823.

Amand, L. E.; Lyngfelt, A.; Karlsson, M.; Leckner, B. Fuel Loading of a Fluidized Bed; Report A 97-221; 1999.

Amand, L. E.; Leckner, B.; Dam-Johansen, K. Influence of SO_2 on the NO/N_20 chemistry in fluidized bed combustion. *Fuel* **1993,** 557–564.

Andersson, B. A. Effects of bed particle size on heat transfer in circulating fluidized bed boilers. *Powder Technology* **1996,** 239–248.

Blankinship, S., Ed. CFB: Technology of the Future? *Power Engineering* **2008,** *2*. https://www.power-eng.com/2008/02/01/cfb-technology-of-the-future/#gref.

Ding, J.; Gidaspow, D. A bubbling fluidization model using kinetic theory of granular flow. *AIChE Journal* **1990,** *36*, 523–538.

Gao, X.; Li, T.; Sarkar, A.; Lu, L.; Rogers, W. A. Development and Validation of an Enhanced Filtered Drag Model for Simulating Gas-Solid Fluidization of Geldart A Particles in All Flow Regimes. *Chemical Engineering Science* **2018,** *184*, 33–51.

Johnsson, F.; Leckner, B. Vertical Distribution of Solids in a CFB Furnace. Proceedings of the 13th International Conference on Fluidized Bed Combustion, 1995; pp. 671–679.

Leckner, B.; Amand. L. Emissions from co-combustion of coal, wood and sludge in CFB. Proceedings of the 8th China-Japan Symposium on Fluidization. Gifu, Japan, 2003; p. 28–35.

Li, T.; Rogers, W. A.; Syamlal, M.; Dietiker, J. The NETL MFiX Suite of multiphase flow models: A brief review and recent applications of MFiX-TFM to fossil energy Technologies. Chemical Engineering Science **2017,** *169*, 259–272.

Musser, J.; Carney, J. *Theoretical Review of the MFIX Fluid and Two-Fluid Models*; DOE/NETL-2020/2100; NETL Technical Report Series, U.S. Department of Energy, National Energy Technology Laboratory, Morgantown, WV, 2020.

Nevalainen, H.; Jergoroff, M.; Saastamoinen, J.; Tourunen, A.; Jantti, T.; Kettunen, A.; Johnsson F.; Niklasson, F. Firing of coal and biomass and their mixtures in 50 kW and 12 MW circulating fluidized beds – Phenomenon study and comparison of scales. *Fuel* **2007,** 2043–2051.

Peters, N. Premixed Burning in Diffusion Flames - the flame zone model of Libby and Economos. *International Journal of Heat and Mass Transfer* **1979,** *22*, 691–703.

Westbrook, C. K.; Dryer, F. L. Simplified Reaction Mechanisms for the Oxidation of Hydrocarbon Fuels in Flames. *Combustion Science and Technology* **1980,** 31–43.

Zhang, W.; Johnsson, F.; Leckner, B. Fluid-dynamic boundary layers in CFB boilers. *Chemical Engineering Science 50.2* **1995,** 201–210.

This page intentionally left blank.

Brian Anderson, Ph.D.
Director
National Energy Technology Laboratory
U.S. Department of Energy

Bryan Morreale
Executive Director
Research & Innovation Center
National Energy Technology Laboratory
U.S. Department of Energy

John Wimer
Associate Director
Strategic Planning
Science & Technology Strategic Plans
& Programs
National Energy Technology Laboratory
U.S. Department of Energy